Simulation of Particle Separation on an Inclined Electric Curtain

Jennifer K.W. Chesnutt
Dept Mechanical Engineering
One UTSA Circle
Univ of Texas at San Antonio
San Antonio, TX 78249-0670
U.S.A.
Jennifer.Chesnutt@utsa.edu

Jeffrey S. Marshall
School of Engineering
The University of Vermont
33 Colchester Blvd.
Burlington, VT 05405
U.S.A.
jmarsha1@uvm.edu

***Abstract* -- Electric curtains have been shown in experiments to successfully remove charged dust particles from a surface using phase-modulated oscillating electric fields on parallel electrodes. Experimental limitations on charge and velocity measurement of individual particles have restricted understanding of the physical mechanism of this phenomenon. A discrete-element method for simulating particle motion in electric curtains is discussed and applied to study particle motion induced by an upward traveling wave on an inclined electric curtain. The upward particle motion induced by the traveling wave is opposed by downward gravitational motion. Particles are influenced by van der Waals adhesion and electrostatic interaction, both to the surface and to each other. These different effects result in a complex particle flow that sometimes leads to separation of particles of different sizes, but in other cases leads to particles moving together in one direction.**

Index Terms-- **Discrete-element method; Electric curtain; Electrostatic processes; Particle separators; Separation processes**

I. Introduction

Particle separation is a key process in a wide range of engineering, agricultural and mining applications. Standard mechanical separation approaches, such as centrifuging or sieving, exhibit poor performance for charged particles, since the electric charges cause the particles to agglomerate to each other or adhere to the vessel walls. This is particularly a problem for small particles, or size about 10μm or less, for which electrostatic charges can easily dominate over gravity or inertial forces.

Electric curtain technology presents an attractive alternative approach for separation of charged particles, since the particle transport method is directly related to the particle charge [1-6]. An electric curtain is constructed from a series of parallel electrodes embedded in a dielectric material and coated by a thin dielectric film. The electrodes have a high-amplitude oscillating electrostatic potential with prescribed phase difference between neighboring electrodes, creating a traveling electrostatic wave that travels up the electric curtain. Electric curtains have long been studied as effective devices for removal of charged dust particles from a surface [7-14], since the transport speed of the dust particles increases with increase in particle charge. Electric curtains have been used for controlled transport of toner particles in photocopier machines [15-17]. Most recently electric curtains have been proposed for particle mitigation in space exploration of dusty planets and planetary bodies, such as the moon and Mars [18-22]. In such applications, the electric curtain could provide an effective method for removal of charged particles from solar panels, space suits, etc.

Use of an electric curtain for separation of particles with different sizes or charges was suggested by Weiss and Thibodeaux [1] with application to sorting of seeds from by-products in agricultural processes. Early work was also reported by Yen and Hendricks [23] on inclined electric curtains; however, their experiments contain only the electrode wires, with no dielectric materials, so many of the particles simply fell through the curtain. Masuda et al. [2] applied the electric curtain for separation by size and charge for particles suspended in a liquid. The effect of electrode geometry on separation efficiency was examined by Machowski and Balachandran [3,4]. A variety of technologies are described by Kawamoto [6] that utilize electric curtains for separation of particles of different size, including an inclined electric curtain, an inclined tube-shaped electric curtain, a spiraling electric curtain, and a roller separation system. In the inclined electric curtain, Kawamoto observes that large particles fall to the bottom of the curtain due to gravity but that smaller particles are carried upward to the top of the curtain.

A number of computational studies have also been performed for electric curtain particle transport. Computational studies of non-adhesive particle motion on an electric curtain are given by Gartstein and Shaw [24] and Kawamoto et al. [14] using a hard-sphere discrete-element method, which by construction can account for particle collisions involving no more than two particles not touching the dielectric surface. This method was applied to an inclined electric curtain by Kawamoto [6]. A soft-sphere discrete-element method for motion of adhesive particles on an electric curtain was developed by Liu and Marshall [25], which can account for collisions involving two or more particles that may also be touching the dielectric surface. This method was used to examine effects of particle collision and adhesion on transport on a horizontal curtain and was later applied to study particle motion under a standing wave electric curtain [26].

The current paper applies the soft-sphere discrete-element method developed in [25] to particle separation on an inclined electric curtain, with an upward-propagating four-phase traveling electric field wave. For this problem, large particles are expected to fall downward under the action of gravity and very small particles are expected to adhere to the dielectric surface. The upward transport of particles by the electric curtain is therefore dominated by a middle-size range of particles. Since particles of different sizes are traveling in different directions, collisions between particles can also play a significant role in determining whether particles are separated by size or all swept in one direction. The computations focus on exploring the effects of adhesion and collision on this system.

II. Computational Method

The electric curtain consists of a periodic array of strip electrodes of width D embedded within a dielectric material of permittivity ε_d. The electrodes have infinite length, with the symmetry axes of adjacent electrodes separated by a distance L. The electrodes are embedded a distance H from the top surface of the dielectric material, which is inclined by an angle θ from the orthogonal plane to the gravitational force (Figure 1). The electrodes are powered by a four-phase rectangular AC voltage to generate a traveling wave that propagates from left to right, up the inclined surface. Particles with diameter d_p, permittivity ε_p, and density ρ_p are positioned on the surface above the dielectric material in an atmosphere with permittivity ε_f, density ρ_f, and viscosity μ.

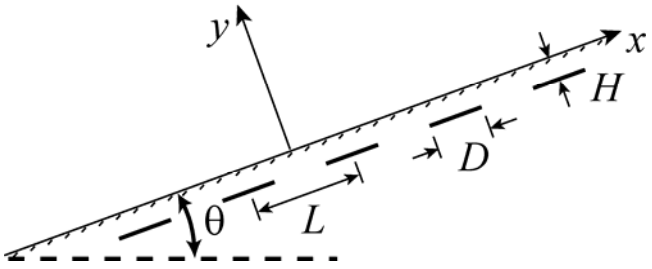

Fig. 1. Schematic diagram showing geometry of electrode array.

A discrete-element method (DEM) similar to that of Marshall [27] is utilized to model collision and adhesion of particles and to model fluid forces and torques on particles. The normal collision force of a particle results from a combination of elastic repulsion, viscous dissipation, and van der Waals adhesion. The combined elastic and van der Waals forces are modeled by the well-known Johnson-Kendall-Roberts theory [28] with particles assumed to be perfectly spherical before contact. The dissipation force is given by an expression of Tsuji et al. [29]. Resistance to rolling of one particle over another particle is modeled through a rolling resistance torque resulting from particle adhesion given by Dominik and Tielens [30]. Resistance to sliding and twisting of adhesive particles is also included in the model [27]. The fluid above the dielectric surface is stationary, with the particles experiencing a fluid drag force given by the classics Stokes expression and a viscous torque.

The interaction of particles within an electric field is modeled assuming each particle possesses a point charge and an induced point dipole located at the particle centroid. The electric field induced by the particles is solved using an optimized multipole expansion approach [31]. Particle images are induced across the dielectric surface using the analytic solution of Sometani [32]. The electric field exerted by the electrodes and dielectric material is generated by first decomposing the AC potential in time and then using a two-dimensional boundary-element method [25, 31]. Particles are subject to a Coulomb force $\mathbf{F}_c = Q\mathbf{E}$ and a dielectrophoretic force $\mathbf{F}_p = \mathbf{p}\cdot\nabla\mathbf{E}$, where Q is the particle charge and $\mathbf{p}$ is the induced dipole moment on the particle, which is proportional to the electric field $\mathbf{E}$ [33].

The computational domain for the DEM simulations consists of four electrodes, having length λ in the x-direction (the direction in which the wave travels), height 2λ in the y-direction, and width 0.5λ in the z-direction (spanwise), where λ is the wavelength of the traveling wave. Both the electric field and the particle motion are assumed to be periodic in x and z. The boundary-element calculations are performed by including five periods in the x-direction on each side of the computational domain for the electric field computation. Each electrode is discretized by 200 evenly distributed line elements and the dielectric surface by 800 evenly distributed line elements for the boundary-element calculations. Following inversion of the boundary-integral equations to obtain the surface sheet charge density on the electrodes and the dielectric surface, the electric field is computed on a two-dimensional uniform grid covering the x-y plane in the computational domain with 801 and 1601 computational points in the x- and y-directions, respectively. In DEM simulations, values of this pre-computed electric field are linearly interpolated onto the centroid of each particle to calculate the Coulomb and dielectrophoretic forces induced by the curtain.

All DEM computations are performed in three dimensions with 1250 particles, and with ratio of particle diameter to wavelength d_p/λ between 0.000625 and 0.003125. For simulations with two particle sizes, the number of particles of each size is chosen to give the same particle volume concentration for each particle size. To calculate the inter-particle Coulomb and dielectrophoretic forces, one period of the particles and their images in each of the x- and z-directions on each side of the domain is used. Each particle is assigned a fixed charge, with tribocharging assumed to be negligible during the simulation due to the relatively short simulation time interval. Particle charge is calculated from a constant value of the particle charge surface density q, such that the net particle charge increases with the square of the particle radius. Particles are initially placed in a single layer on the dielectric surface in a lattice formation with approximately equal spacing in the x- and z-directions, and are then given a small random perturbation in each of the x- and z-directions.

Results are nondimensionalized for ease of numerical analysis using characteristic scalings for length (λ) and time ($1/f$), where f is wave frequency. The normalized particle velocity component is $u' = u/f\lambda$ and particle elevation height is $y' = y/\lambda$. Each particle has a fixed charge. Particles are subject to van der Waals adhesion with each other and with the dielectric surface, with adhesion characterized by the critical adhesion force between two particles of the same radius $F_{crit} = 3\pi\gamma\, r_p/2$, where r_p is particle radius and γ is the effective adhesive surface energy density of the two particles [28]. To measure the relative importance of the adhesion force to the electrostatic force, a dimensionless adhesion parameter Φ is defined as

$$\Phi = \frac{F_{crit}}{E_0 Q_0} = \frac{3\pi\gamma\, r_0}{2E_0 Q_0}, \qquad (1)$$

where r_0 is nominal particle radius, Q_0 is nominal charge, $E_0 \equiv \phi_{PP}/G$ is a measure of the electric field strength, ϕ_{PP} is peak-to-peak voltage change, and $G = L - D$ is the gap width between two neighboring electrodes. Values for all parameters are given in Table 1 for an example case with two particle sizes. All cases utilize these parameter values with the exception that particle radii, adhesion parameter, and inclination angle may vary, being explicitly stated for other cases.

TABLE 1
PARAMETER VALUES FOR SIMULATIONS WITH TWO PARTICLE SIZES AND ADHESION

Parameter	Value	Unit
Particle radius 1, r_{p1}	15	μm
Particle radius 2, r_{p2}	20	μm
Particle density, ρ_p	3520	kg/m^3
Particle relative permittivity, $\varepsilon_p/\varepsilon_f$	3	
Fluid viscosity, μ	1.8×10^{-5}	kg/m·s
Fluid density, ρ_f	1.2	kg/m^3
Nominal particle radius, r_0	1	mm
Nominal charge, Q_0	10^5	Elementary charges
Particle charge surface density, q	-3.05×10^{-6}	C/m^2
Electrode width, D	1	mm
Electrode separation, L	2	mm
Electrode embedded depth, H	40	μm
Wave length, λ	8	mm
Wave frequency, f	10	Hz
Electrode voltage (peak-to-peak), ϕ_{PP}	1600	V
Relative permittivity of dielectric material, $\varepsilon_d/\varepsilon_f$	1.3	
Adhesion parameter, Φ	5×10^{-4}	
Inclination angle, θ	20	deg
Computational domain $X \times Y \times Z$	8×16×4	mm

III. Results With No Particle-Particle Interactions

The effects of inclination angle of the dielectric surface and particle size on particle transport are first investigated through computations with particles of one size with an adhesion parameter $\Phi = 0$. Electrostatic interactions between different particles and between particles and the dielectric surface are neglected. Particle-particle collisions are also neglected, but particles collisions with the dielectric surface are included. These results provide a baseline with which to evaluate the effects of particle-particle interactions and adhesion in Sections IV and V.

Figure 2 shows results for measures of particle transport as a function of the particle radius, ranging from 5-25 μm, for cases with different inclination angle. Data are given for the particle velocity u' and elevation y', both of which are averaged in time and averaged over all particles of the same size. The error bars in the plot denote the standard deviation of the particle velocity and elevation height from the averaged values. For zero inclination angle, the average particle propagation velocity increases with particle radius, ranging from less than 10% of the wave speed ($f\lambda$) for $r_p = 5$ μm to about 80% of the wave speed for $r_p = 25$ μm. As the curtain inclination angle is increased, the particles have small, or even slightly negative, propagation velocity for small particle radii ($r_p \le 15$ μm) but then increasing propagation velocity up the curtain for larger particle sizes. Movies of the particle velocities for these cases show particles being pushed up the electric curtain by the electrode potential oscillations with the upward wave motion, but then falling downward due to gravity once the particles are levitated a sufficient distance away from the curtain surface. For the largest inclination angle ($\theta = 40°$), the particle velocity is oriented down the curtain for all particle radii, and the speed that the particles fall downward in fact increases as the particle radius increases. For a given particle radius, particle velocity decreases as inclination angle increases in most cases, as expected.

The averaged particle elevations shown in Fig. 2b range between 4-20% of the curtain wavelength λ. In all cases the average elevation is significantly larger than the particle radius (for which r_p/λ varies between 0.0006 and 0.003), indicating that all cases exhibit a significant amount of particle displacement off the dielectric surface. There is no general trend between particle elevation and either the inclination angle or the particle radius. However, at the largest particle radius considered ($r_p = 25$ μm) the average elevation increases with increase in inclination angle, varying from $y' = 0.07$ for $\theta = 0°$ to $y' = 0.19$ for $\theta = 40°$.

Examples showing the relationship between the instantaneous velocity (u') and the instantaneous elevation (y') of a single particle, nondimensionalized by the wave speed and the wavelength, respectively, are shown in Fig. 3 for cases with $\theta = 0°$, 20°, 30° and 40°. In each plot, the velocity is given on the upper curve and labeled on the left-hand axis and the elevation is given on the lower curve and labeled on the right-hand axis. The particle velocity in these

figures exhibits a rapid variation, with frequency of approximately four times the wave frequency, during which the velocity alternates between positive and negative values. The time scale of these oscillations corresponds to the time required for the neighboring electrode to change sign of its electrostatic potential if it is assumed that a particle moves by one electrode during each oscillation. The positive velocity corresponds to the initial push of the particle toward the neighboring i+1 electrode due to the sign change of the ith electrode, and the negative velocity is caused by the backward pull that occurs when the particle overshoots the i+1 electrode. The particle motion during these rapid oscillations occurs by rolling on the surface and by small hops from one electrode to the next, with particle elevation $y' < 0.1$.

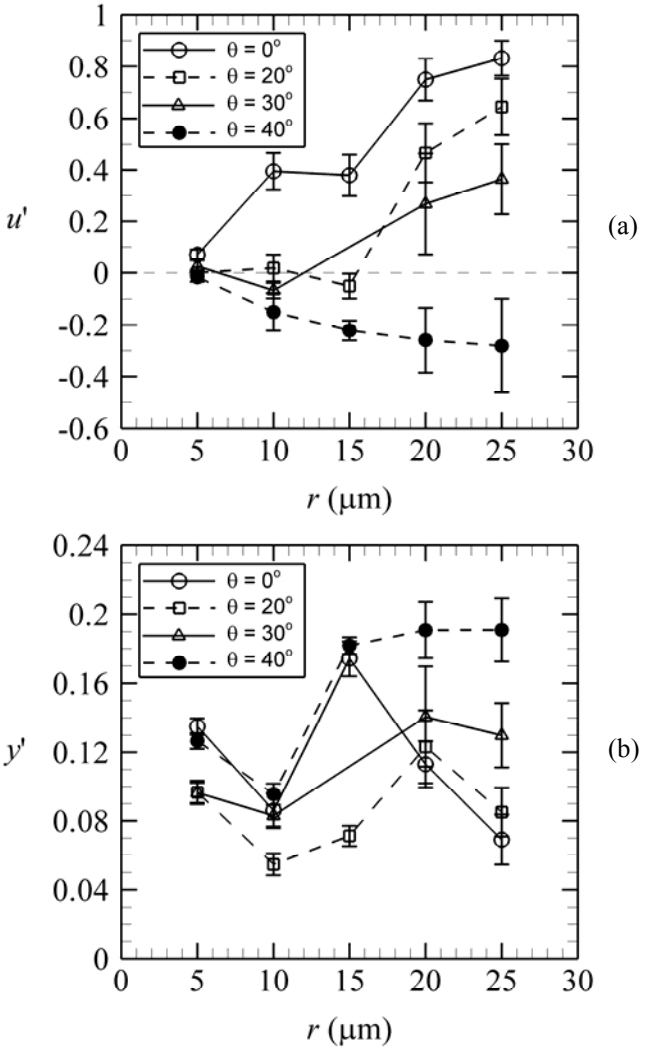

Fig. 2. Transport properties versus particle radius for different values of inclination angle (θ), including (a) time-averaged particle transport velocity and (b) time-averaged particle elevation, both averaged over all particles of the same size. All runs have no particle adhesion and no particle-particle interactions.

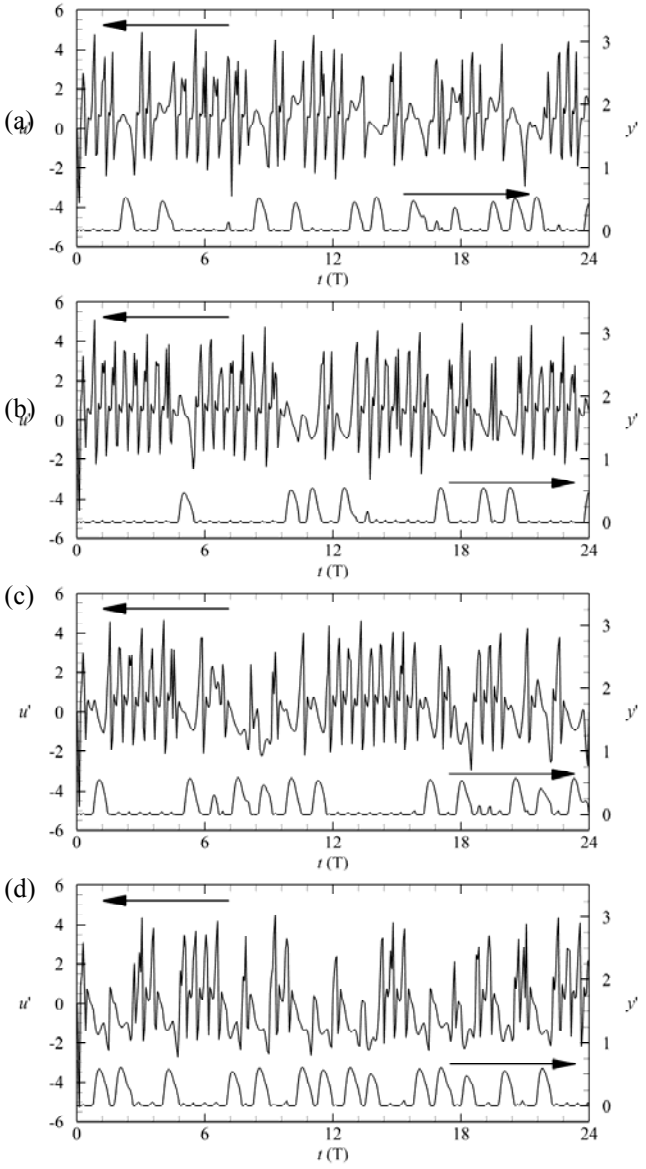

Fig. 3. Time variation of the transport velocity (left) and elevation (right) of a single particle, with time normalized by wave period T, velocity normalized by wave speed, and height normalized by wavelength, for inclination angles of (a) 0°, (b) 20°, (c) 30°, and (d) 40°. All runs have particle radius 20μm and no particle adhesion.

In addition to the rapid oscillations in Fig. 3 is observed intermittent periods during which the particle exhibits much larger hops, lasting approximately half of the wave period and with particle elevation y' significantly greater than 0.1. The particle velocity does not oscillate rapidly during these larger hops, but it instead exhibits a gradual variation throughout the hop interval. For the lower two values of curtain inclination ($\theta = 0°$ and 20°) the particles tend to have positive velocity during these larger hops, whereas for the highest inclination value ($\theta = 40°$) the larger hops tend to coincide with negative particle velocity. Both positive and

negative velocities are observed during the large hops for the $\theta = 30°$ case.

An example showing particle positions at a fixed time $t' = 24$ for a case with $\theta = 0°$ and $r_p = 20\,\mu\text{m}$ is given in Fig. 4. Electrodes are centered at $x' = -3$, -1, 1 and 3 underneath the dielectric surface. Although all particles are initialized in random positions on the dielectric surface, the particles are transported in such a way as to form sheets that are advected together, each resulting from a given change in electrode potential. The figure shows two distinct regions of particle motion. There is a region of particles gathered at the two positively-charged electrodes on the curtain, with a small bridge of particles spanning the two electrodes. Particles in this region are exhibiting the small hopping motion. Then there are sheets of particles much further away from the dielectric surface, which are thrust far away from the surface and then settle slowly back down to the surface. These particles are exhibiting the larger hopping motion.

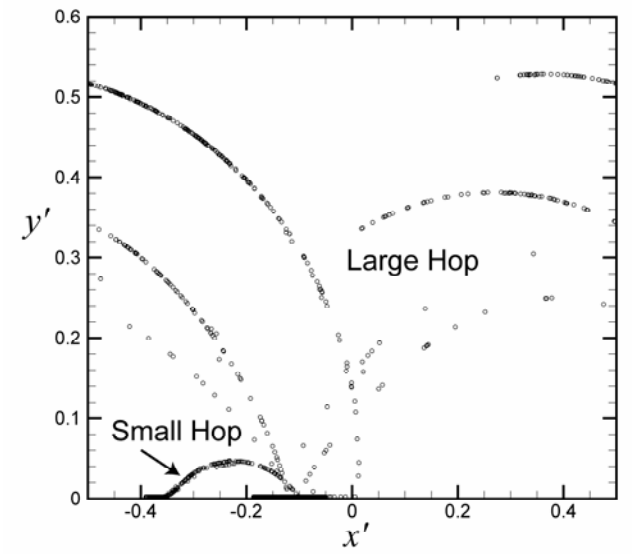

Fig. 4. Plot showing particle positions along the electric curtain at time $t' = 24$ for a case with $\theta = 0°$ and 20μm particle radius.

IV. Results With Particle-Particle Interactions and No Adhesion

A study of the effect of particle-particle interaction on particle transport on the electric curtain was performed for cases with inclination angles $\theta = 0°$ and 20° and particle radii $r_p = 15\,\mu\text{m}$ and 20μm. Two different types of computations are performed. The first computation is for a mixture of particles of the two sizes, with the same volume concentration for each size. This computation includes particle interactions with each other and with the dielectric curtain, including both particle-particle collisions and particle electrostatic interactions. The second type of computation (the control) neglects these particle interactions, so that the motion of the particles of the two different sizes is the same as if the other particles were not present. Adhesion of particles to each other and to the dielectric surface is neglected in both computations. Results of the comparison for the averaged particle velocity and elevation are shown in Fig. 5.

Computations with a horizontal curtain ($\theta = 0°$) shown in Figs. 5a-b indicate that the average transport velocity of the particles is nearly the same with and without particle interactions, although the difference between the speeds of the two particle sizes decreases with the particle interactions, as would be expected in the presence of collisions. The average particle elevation is lower with particle interactions than without interactions for both particle sizes. The decrease in particle elevation is primarily due to the dielectrophoretic (DEP) interaction between each particle and its image over the dielectric surface, which is not included in the first set of computations but is included in the second set. The DEP force induced by the particle image pulls the particles downward toward the dielectric surface.

Computations with an inclined curtain ($\theta = 20°$) indicate that particle-particle interactions have can be significantly influenced by gravitational force in the direction opposite that of the wave motion. With no particle-particle interaction, the smaller $r_p = 15\,\mu\text{m}$ particles have almost no net velocity on the curtain, with the upward wave velocity nearly balanced by the downward gravitational velocity. The larger $r_p = 20\,\mu\text{m}$ particles have an upward velocity equal to about half the electrostatic wave speed. In the presence of particle-particle interactions, the smaller particles are observed to have a positive velocity up the curtain and the larger particles are observed to have a negative velocity down the curtain, thus giving rise to a separation of particles by size. The average particle elevation similarly increases for the smaller particles and decreases for the larger particles in the presence of particle-particle interactions.

For most computations with particles of a single size, the particle motion as examined in movies and in plots of the time variation of transport velocity and elevation averaged over the particles exhibits a short transient period lasting about five wave periods followed by a repeating particle transport pattern with oscillations that are either equal to or a multiple of the electric curtain oscillation period. During the period following the initial transient, the particle velocities (averaged over all particles) exhibit fairly regular time oscillations, as illustrated in Fig 6b for a case with $r_p = 20\,\mu\text{m}$ and $\theta = 20°$. Both the small and large hopping motion described in Section III and shown in Fig. 4 are observed for these computations. In contrast to the normal case, the computation with $r_p = 15\,\mu\text{m}$ and $\theta = 20°$ (and no particle interactions) shown in Fig 6a does not exhibit regularly oscillating particle velocity, but rather the particle motion appears to intermittently pass into and out of different modes of motion as the computation progresses, resulting in a very irregular curve in Fig 6a for time variation of particle velocity. The time period associated with velocity oscillations in this case is approximately twice that observed for the other cases examined. The small and large hopping motion described with reference to Fig 4 is also not observed for this case, but instead the particles are observed to

oscillate more slowly back and forth. This case gives an example of a period-doubling bifurcation of the particle motion on the electric curtain, wherein particles suddenly transition from one mode to a very different mode of motion, with similar transitions in average particle transport velocity and elevations.

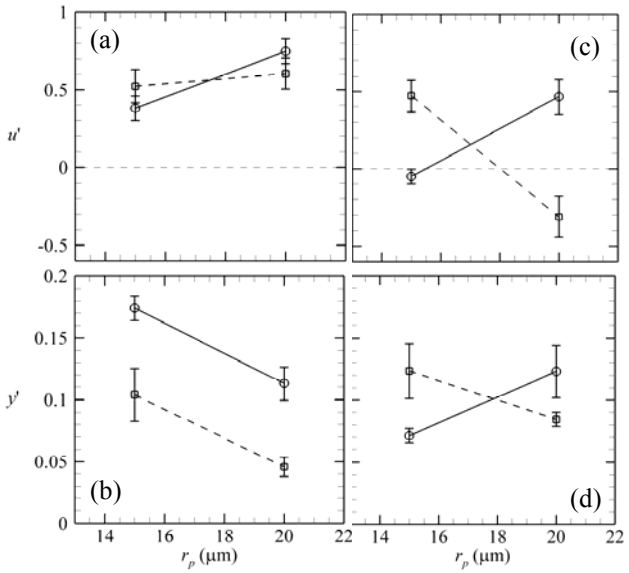

Fig. 5. Transport properties versus particle radius including (a) time-averaged particle transport velocity (u') averaged over particles of the same size, for $\theta = 0°$, (b) time-averaged particle elevation (y') averaged over all particles of the same size, for $\theta = 0°$, (c) u' for $\theta = 20°$, and (d) y' for $\theta = 20°$. Cases include computations with a single particle size without particle-particle interactions (circles, solid line) and computations with two different particle sizes with particle-particle interactions (squares, dashed line). All runs have no particle adhesion.

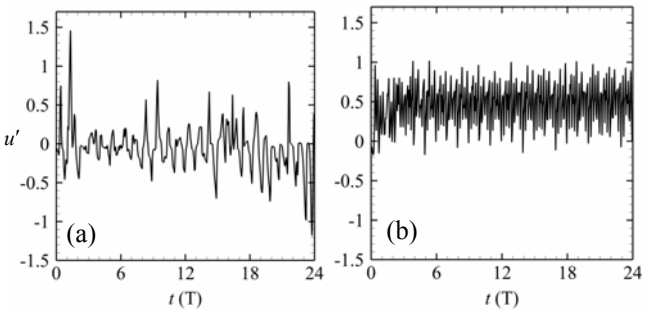

Fig. 6. Time variation of the particle velocity averaged over all particles for a case with no particle interaction and $\theta = 20°$, for (a) 15μm and (b) 20μm radius particles.

Plots showing particle positions at a fixed time for the case with particle-particle interactions are given in Fig. 7 for the x-y and x-z planes. Blue and red coloring is used to denote particles with radii of 15 and 20μm, respectively. It is observed in Fig. 7a that even very late in the computation, the particles are observed to form sheets, where each sheet consists of particles of only one size. For this computation, the sheets formed of smaller particles extend upwards to a higher elevation than do those formed of the larger particles, which is consistent with the average elevation values recorded in Fig. 5d. The smaller particles tend to be attracted more quickly to the positively-charged electrodes than are the larger particles, as is apparent in Fig. 7b. Consequently, the small particles for this case tend to move forward in short hops from one electrode to the next, whereas the larger particles tend to be thrown upward and gradually settle downwards on the curtain, traveling slowly in the negative x-direction.

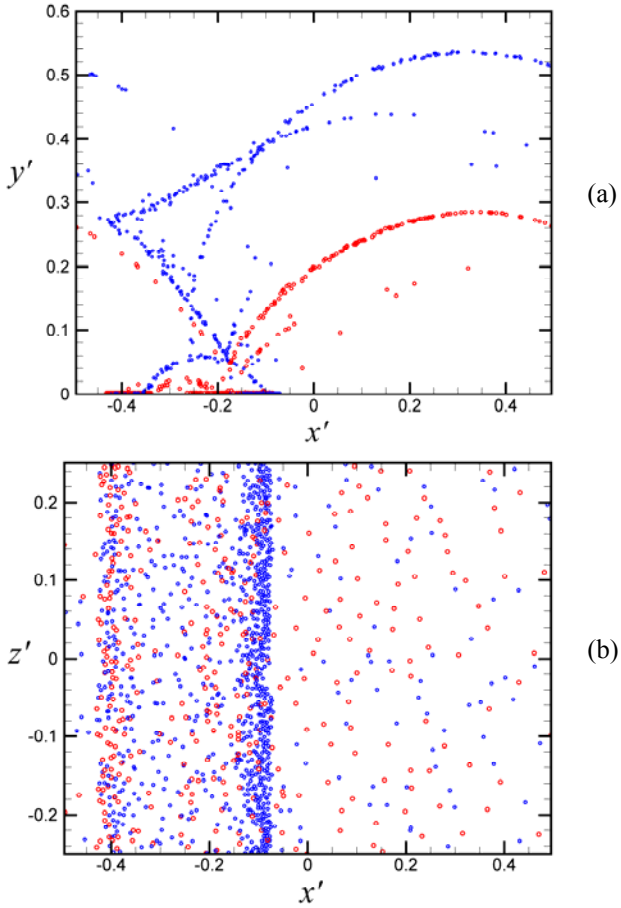

Fig. 7. Plots showing particle positions along the electric curtain at time $t' = 24$ for a case with $\theta = 20°$ in the (a) x-y and (b) x-z planes, showing particles with radii of 15μm (blue) and 20μm (red).

As can be seen from Figs. 5c-d and the mode transition observed in Fig. 6, the dynamics of interacting particles of different sizes on an inclined electric curtain is highly complex and sometimes results in non-intuitive consequences. The particles exhibit numerous regimes under the combined influence of the forward-propagating electrostatic wave, the downward effect of gravity, and the interactional effects of the other particles. In some cases this results in particles hopping forward with the traveling wave, in others the particles are thrust far outward from the dielectric surface and drift either gradually in the upward direction under the electrostatic field or gradually downward due to gravity. In a number of cases we observe particles to slosh back and forth in a periodic manner between a small set of electrodes, first advancing forward with the traveling

wave and then falling backward under gravity. Moreover, particles are sometimes observed to be transported in one mode for a period of time, and then to unexpectedly switch into a different mode.

V. Results With Particle-Particle Interactions with Adhesion

A second study was performed to examine the effects of particle adhesion on transport on the electric curtain. Two different computations were again conducted, both for the case with $\theta = 20°$ and with a mixture of particles with radii $r_p = 15\,\mu\text{m}$ and 20μm. Both computations included all particle electrostatic interactions and collisions; however the first computation neglected particle adhesion whereas the second computation included adhesion, with adhesion coefficient set to $\Phi = 5 \times 10^{-4}$.

As shown in Fig. 8, both computations give about the same average elevations for both particle sizes. The case with adhesion results in a slight decrease of the average particle velocity for the smaller 15μm particles and a more substantial change in velocity of the larger 20μm particles. In the latter particle size, the computation with adhesion changed the average velocity from a negative value of about 30% of the wave speed to a positive value of about 10% of the wave speed. For both particles sizes, the reduction in absolute value of the particle velocity is consistent with the expected tendency of adhesion to decrease the frequency of particle hops due to the increased force from adhesion holding the particles to the surface. As discussed with reference to Fig. 3, much of the particle net motion occurs during the large intermittent hops, so reduction in hop frequency leads to a reduction in the average particle transport velocity, either in the backward or forward directions. This reduction in hop frequency is also supported by the slight reduction in average elevation with particle adhesion for 20μm particles. For 15μm particles, there was a large standard deviation in elevation between different particles which makes any difference in average elevation with inclusion of adhesion difficult to distinguish.

VI. Conclusions

A numerical study has been conducted of the effect of particle size and various types of particle interactions on inclined electric curtains. The computations used a soft-sphere discrete-element method to model motion of either adhesive or non-adhesive particles in the presence of an electrostatic field. The shape of the electrodes and design of the curtain was accurately captured using a boundary-element method for the electric field. Particle electrostatic interactions with each other are approximated by treating each particle as both an electric source and a dipole. The simulations show that net particle transport takes place primarily during intermittent hops of the particles off of the dielectric surface. The velocity magnitude and direction during these hops changes as a function of both the curtain inclination and the particle size. Particle electrostatic interaction with their image over the dielectric surface causes a decrease in average particle elevation height. Collisions between particles cause the velocity difference between particles of two different sizes to decrease. Particle adhesion to the dielectric surface causes a decrease in hopping frequency, with resulting decrease in magnitude of the average particle transport velocity.

The inclined electric curtain has the potential to function as an effective separation device for charged particles, which are often difficult to separate using other methods. Generally it is found that larger particle sizes have a higher velocity up the curtain, until some critical size is reached where the gravitational force dominates and particles fall back downward. However, in the presence of electric curtain inclination, the combined effects of gravity, electrostatic wave forces, adhesion, collisions and particle-particle and particle-surface electrostatic interactions leads to a highly complex system, with sometimes unexpected results.

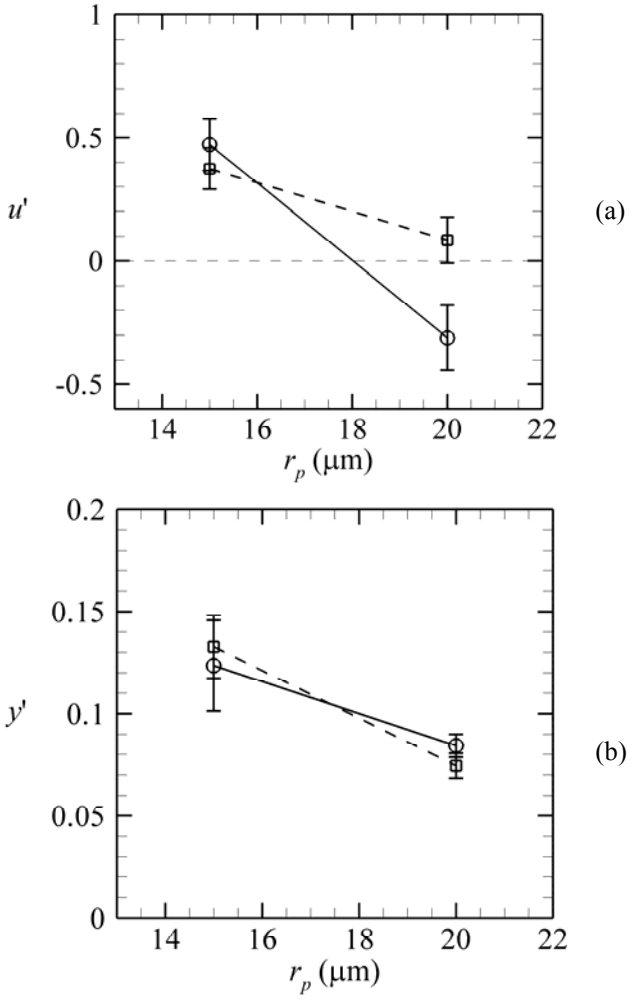

Fig. 8. Transport properties versus radius for cases with two different particle sizes and particle-particle interactions including (a) time-averaged particle transport velocity and (b) time-averaged particle elevation, both averaged over all particles of the same size. Computations are reported both without particle adhesion (circles, solid line) and with particle adhesion (squares, dashed line). All runs are for $\theta = 20°$.

ACKNOWLEDGMENT

This work has been supported by NASA under cooperative agreement number NNX08AZ07A. Dr. Carlos Calle serves as the NASA liaison. We also acknowledge financial support from Vermont EPSCoR (EPS 0701410) and National Institutes of Health (T32 HL04776-29).

REFERENCES

[1] L. C. Weiss and D. P. Thibodeaux, "Separation of seed by-products by an AC electric field," *Journal of the American Oil Chemists' Society*, vol. 61, no. 5, pp. 886-890 (1984).

[2] S. Masuda, M. Washizu, and M. Iwadare, "Separation of small particles suspended in liquid by non-uniform traveling field," *IEEE Transactions on Industry Applications*, vol. IAA-23, pp. 474-480 (1987).

[3] W. Machowski and W. Balachandran, "Electrodynamic control and separation of charged particles using traveling wave field technique," *Journal of Electrostatics*. vols. 40-41, pp. 325-330 (1997).

[4] W. Machowski, W. Balachandran, and D. Hu, "Influence of electrode geometry on transport and separation efficiency of powders using traveling wave field technique," IEEE/IAS Annual Meeting, Orlando, Florida, U.S.A., Conference Records, vol. 2, pp. 1302-1309 (1995).

[5] H. Kawamoto and N. Hasegawa, "Traveling wave transport of particles and particle size classification," *Journal of Imaging Science and Technology*, vol. 48, no. 5, pp. 404-411 (2004).

[6] H. Kawamoto, "Some techniques on electrostatic separation of particle size utilizing electrostatic traveling-wave field," *Journal of Electrostatics*, vol. 66, pp. 220-228 (2008).

[7] S. Masuda, K. Fujibayashi, K. Ishida, H. Inaba, "Confinement and transportation of charged aerosol clouds via electric curtain," *Electrical Engineering in Japan*, vol. 92, pp. 43-52 (1972).

[8] M. Onozuka, Y. Ueda, Y. Oda, K. Takahashi, Y. Seki, I. Aoki, S. Ueda, and R. Kurihara, "Development of dust removal system using static electricity for fusion experimental reactors," *Journal of Nuclear Science and Technology*, vol. 34, pp. 1031-1038 (1997).

[9] Z. Dudzicz, "The path of oscillation of dust particles in the field of the electric curtain of the plane type supplied with AC voltage," *Journal of Electrostatics*, vol. 23, pp. 207-214 (1989).

[10] Z. Dudzicz, "Electrodynamics of charged dust particles and repulsion force within plane-type electric curtain," *Journal of Electrostatics*, vol. 51-52, pp. 111-116 (2001).

[11] Z. Dudzicz, "Recording of dust particle oscillation path inside electric curtain by laser diode apparatus," *Optica Applications*, vol. XXXV(4), pp. 907-912 (2005).

[12] J. M. Hemstreet, "Three-phase velocity distribution of Lycopodium particles on the Masuda panel," *Journal of Electrostatics*, vol. 27, pp. 237-247 (1992).

[13] J. M. Hemstreet, "Velocity distribution on the Masuda panel," *Journal of Electrostatics*, vol. 17, pp. 245-254 (1985).

[14] H. Kawamoto, K. Seki, and N. Kuromiya, "Mechanism of traveling-wave transport of particles," *Journal of Physics D: Applied Physics*, vol. 39, pp. 1249-1256 (2006).

[15] J. R. Melcher, E. P. Warren, and R. H. Kotwal, "Traveling wave delivery of single component developer," *IEEE Transactions on Industry Applications*, vol. 25, pp. 956-961 (1989).

[16] F. W. Schmidlin, "A new nonlevitated mode of traveling wave toner transport," *IEEE Transactions on Industrial Applications*, vol. 27, pp. 480-487 (1991).

[17] F. W. Schmidlin, "Modes of traveling wave particle transport and their applications," *Journal of Electrostatics*, vol. 34, pp. 225-244 (1995).

[18] C.I. Calle, M.K. Mazumder, C.D. Immer, C.R. Buhler, J.S. Clements, P. Lundeen, A. Chen, and J.G. Mantovani, "Controlled particle removal from surfaces by electrodynamic methods for terrestrial, lunar and Martian environmental conditions," Journal of Physics: Conference Series, vol. 142, 012073 (2008).

[19] C. I. Calle, C. R. Buhler, J. L. McFall, and S. J. Snyder, "Particle removal by electrostatic and dielectrophoretic forces for dust control during lunar exploration missions," *Journal of Electrostatics*, vol. 67, pp. 89-92 (2009).

[20] P. Atten, H. L. Pang, and J. L. Reboud, "Study of dust removal by standing wave electric curtain for application to solar cells on Mars," *IEEE Transactions on Industry Applications*, vol. 45, pp. 75-86 (2009).

[21] R. Sharma, C. A. Wyatt, J. Zhang, C. I. Calle, N. Mardesich and M. K. Mazumder, "Experimental evaluation and analysis of electrodynamic screen as dust mitigation technology for future mars missions," *IEEE Transactions on Industry Applications*, vol. 45, no. 2, pp. 591-596.

[22] M. K. Mazumder, R. Sharma, A. S. Biris, J. Zhang, C. I. Calle, and M. Zahn, "Self-cleaning transparent dust shields for protecting solar panels and other devices," *Particulate Science and Technology*, vol. 25, pp. 5-20 (2007).

[23] A.C. Yen, C.D. Hendricks, "A planar electric curtain used as a device for the control and removal of particulate materials," *Journal of Electrostatics*, vol. 4, pp. 255-266 (1978).

[24] Y. N. Gartstein and J. G. Shaw, "Many-particle effects in traveling electrostatic wave transport," *Journal of Physics D: Applied Physics*, vol. 32, pp. 2176-2180 (1999).

[25] G. Liu and J. S. Marshall, "Effect of particle adhesion and interactions on motion by traveling waves on an electric curtain," *Journal of Electrostatics*, vol. 68, pp. 179-189 (2010).

[26] G. Liu and J. S. Marshall, "Particle transport by standing waves on an electric curtain," *Journal of Electrostatics*, vol. 68, pp. 289-298 (2010).

[27] J. S. Marshall, "Discrete-element modeling of particulate aerosol flows," *Journal of Computational Physics*, vol. 228, pp. 1541-1561 (2009).

[28] K. L. Johnson, K. Kendall, and A. D. Roberts, "Surface energy and the contact of elastic solids," *Proceedings of the Royal Society of London A*, vol. 324, pp. 301-313 (1971).

[29] Y. Tsuji, T. Tanaka, and T. Ishida, "Lagrangian numerical simulation of plug flow of cohesionless particles in a horizontal pipe," *Powder Technology*, vol. 71, pp. 239-250 (1992).

[30] C. Dominik and A. G. G. M. Tielens, "Resistance to rolling in the adhesive contact of two elastic spheres," *Philosophical Magazine A*, vol. 92, pp. 783-803 (1995).

[31] G. Liu, J. S. Marshall, S.-Q. Li and Q. Yao, "Discrete-element method for particle capture by a body in an electrostatic field," *International Journal for Numerical Methods in Engineering*, vol. 84, no. 13, pp. 1589-1612 (2010).

[32] T. Sometani, "Image method for a dielectric plate and a point charge," *European Journal of Physics*, vol. 21, pp. 549-554 (2000).

[33] T. B. Jones, *Electromechanics of Particles,* Cambridge University Press, Cambridge, U.K. (1995).